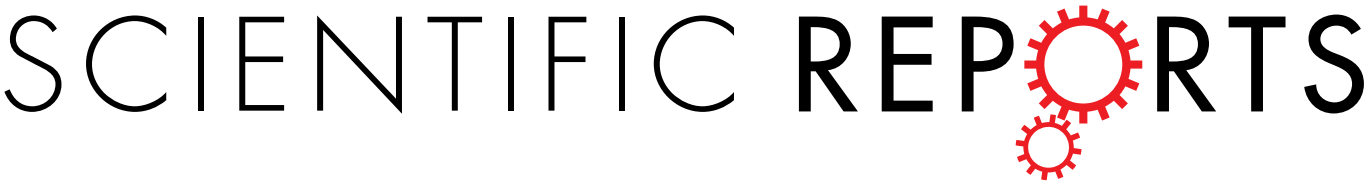

OPEN

Thermodynamic origin of instability in hybrid halide perovskites

E. Tenuta, C. Zheng & O. Rubel

Received: 28 July 2016
Accepted: 01 November 2016
Published: 24 November 2016

Degradation of hybrid halide perovskites under the influence of environmental factors impairs future prospects of using these materials as absorbers in solar cells. First principle calculations can be used as a guideline in search of new materials, provided we can rely on their predictive capabilities. We show that the instability of perovskites can be captured using *ab initio* total energy calculations for reactants and products augmented with additional thermodynamic data to account for finite temperature effects. Calculations suggest that the instability of $CH_3NH_3PbI_3$ in moist environment is linked to the aqueous solubility of the CH_3NH_3I salt, thus making other perovskite materials with soluble decomposition products prone to degradation. Properties of NH_3OHPbI_3, $NH_3NH_2PbI_3$, PH_4PbI_3, SbH_4PbI_3, $CsPbBr_3$, and a new hypothetical SF_3PbI_3 perovskite are studied in the search for alternative solar cell absorber materials with enhanced chemical stability.

The search for cost-effective solar cell absorber materials that can compete with the performance of crystalline silicon and thin-film (GaAs, CdTe and Cu(In, Ga)Se_2) solar cells remains the priority for renewable energy material research. A recently emerged class of hybrid halide perovskite materials holds a promise to lead the way towards low-cost photovoltaic devices as they combine an energy conversion efficiency of nearly 20% with a low-temperature solution processing technology[1–4]. The structure of hybrid perovskites $X^+M^{2+}Z_3^-$ is formed by a combination of various organic cations $X^+ = (CH_3NH_3, NH_4, CH_5N_2)$, metallic cations $M^{2+} = (Pb, Sn)$, and halide anions $Z^- = (I, Cl, Br)$ with $CH_3NH_3PbI_3$ being a prominent example. Perovskite materials possess a unique combination of characteristics that make them useful in photovoltaic applications including a favourable band gap of about 1.5–1.6 eV, efficient optical adsorption, long lifetime of optical excitations, and high level of mobility for charge carries of both polarities[5–8].

A major weakness of perovskite solar cells is degradation of the power conversion efficiency in moist environment[9,10]. This degradation can be observed in $CH_3NH_3PbI_3$ cells through the colour changing from black to yellow accompanied by a noted decreases in absorption and deterioration of the overall cell performance over time[11,12]. The absorbance at 410 nm has been reported to decrease by 50% after 4 hours of exposure to environment with the relative humidity of 98%[12]. The same study linearly extrapolated from the previous result concluded that the identical degradation would take approximately one year at the relative humidity of 20%[12].

Frost *et al.*[13] proposed an acid-base chemistry mechanism to explain the role of water in the degradation process. In this process the decomposition is driven by protic properties of the $[CH_3NH_3]^+$ ion, thus suggesting that aprotic hybrid perovskites (e.g., $(CH_3)_4NPbI_3$) could potentially be more stable[13]. However, this strategy was not confirmed experimentally to the best of our knowledge.

Density functional theory (DFT) simulations of the perovskite-water interface[14,15] provided further insight to kinetics of the degradation mechanism at the atomic scale. Mosconi *et al.*[14] observed dissolution of iodine cage and subsequent release of methylammonium ions as well as incorporation of water molecules in the perovskite structure at the interface. The simulation results reported by Zhang and Sit[15] indicate deprotonation of methylammonium as an initial step in dissolution of the perovskite. Furthermore, first principle calculations[16] performed without taking into account solvent effects suggest that hybrid halide perovskites may be intrinsically unstable. This conclusion is based on a nearly zero enthalpy of reaction associated with decomposition of the perovskite structure, which is evaluated based on the total energy of reactant and products. Frost *et al.*[13] attributed the intrinsic instability of halide perovskites $X^+M^{2+}Z_3^-$ to its relatively low Madelung lattice energy as compared to oxide perovskites that belong to $A^{2+}B^{4+}O_3^{2-}$ family. This result implies that the environmental factors (such as moisture, UV radiation, and elevated temperatures) may only accelerate the decomposition process. Therefore, the effectiveness of encapsulation as a strategy to prevent moisture damage may not guarantee a long-term stability of perovskite solar cells as evidenced by Han *et al.*[17].

Department of Materials Science and Engineering, McMaster University, 1280 Main Street West, Hamilton, Ontario L8S 4L8, Canada. Correspondence and requests for materials should be addressed to O.R. (email: rubelo@mcmaster.ca)

Compound	Lattice parameter (Å)	E_{tot} (eV/f.u.)	$\widetilde{\mu}^{o}_{300\,K}$ (eV/f.u.)
$CH_3NH_3PbI_3$ (solid)	$a=8.92$, $c/a=1.48$[a]	−3146.596	−0.70[54]
PbI_2 (solid)	$a=4.668$, $c/a=1.63$[b]	−2302.282	−0.34[55]
CH_3NH_3I (solid)	$a=5.146$, $c/a=1.86$[c]	−844.266	−0.25[56]
SF_3PbI_3 (solid)	$a=6.546$	−4890.024	~−0.7[d]
H_2O (solid)	$a=4.440$, $c/a=1.63$[e]	−471.805	−0.06[f55,57]
SO_2 (gas)	…	−1157.758	−0.66[55]
HF (gas)	…	−679.866	−0.45[55]
HI (gas)	…	−333.125	−0.55[55]

Table 1. Equilibrium lattice parameters, electronic total energy E_{tot} per formula unit (f.u.), and change in the chemical potential $\widetilde{\mu}^{o}_{300\,K}$ that accounts for the free energy of the compounds at the finite temperature and pressure not captured in DFT total energy. [a]Experimental: $a=8.86$ Å, $c/a=1.43$[58]; other theoretical: $a=8.80$ Å, $c/a=1.48$[59]. [b]Experimental: $a=4.557$ Å and $c/a=1.53$[60]. [c]Experimental: $a=5.11$ Å and $c/a=1.75$[61] [d]The value identical to $CH_3NH_3PbI_3$ is used as an aproximation. [e]Experimental: $a=4.5181$ Å and $c/a=1.63$[62]. [f]The value includes contributions from solid and liquid phases that correspond to −0.05 and −0.01 eV, respectively.

Here we utilize DFT to explore stability of perovskite structures from thermodynamic perspective. We will show that the finite temperature effects, that are omitted in former calculation of stability of $CH_3NH_3PbI_3$[18,19], can play a decisive role when the decomposition reaction takes place in the presence of a solvent and yields a water-soluble product. We will also examine properties of several alternatives, NH_3OHPbI_3, $NH_3NH_2PbI_3$, PH_4PbI_3, SbH_4PbI_3, and $CsPbBr_3$, as well as a hypothetical material, SF_3PbI_3, in a search for perovskite compounds with an enhanced chemical stability for photovoltaic applications.

Results and Discussion

Chemical stability of $CH_3NH_3PbI_3$. We begin by examining the chemical stability of $CH_3NH_3PbI_3$ against decomposition. The structural changes in the course of degradation involve disappearance of X-ray diffraction peaks that are characteristic for $CH_3NH_3PbI_3$ and appearance of PbI_2 peaks[20], which suggests the following reaction (phases)

$$CH_3NH_3PbI_3 \rightleftharpoons PbI_2 + CH_3NH_3I. \tag{1}$$

The standard approach for predicting the direction of a chemical reaction involves evaluation of the change in the Gibbs free energy between reactants and products (see ref. 21, Chap. 7), which can be split into two terms for convenience

$$\Delta G^{o}_{T} = \Delta H^{o}_{0K} + \Delta\widetilde{\mu}^{o}_{T}. \tag{2}$$

Here ΔH^{o}_{0K} is the standard reaction enthalpy change at zero temperature, and $\Delta\widetilde{\mu}^{o}_{T}$ captures finite temperature effects on the chemical potentials of species involved.

The enthalpy change at zero temperature can be readily evaluated based on the DFT total energy calculations

$$\Delta H^{o}_{0K} \approx \sum_{i}^{\text{products}} n_i E_{tot}[i] - \sum_{j}^{\text{reactants}} n_j E_{tot}[j], \tag{3}$$

where n and E_{tot} are the number and the total energy of the chemical species involved in the reaction. It should be noted that the bare DFT total energies in Eq. (3) do not fully capture the standard enthalpy changes at zero temperature as they do not include a zero-point vibrational energy and, less importantly, the standard pressure effects on E_{tot}. Therefore, the relation (3) is approximate. In the case of $CH_3NH_3PbI_3$, the decomposition reaction yields two products: PbI_2 and CH_3NH_3I. The corresponding lattice parameters and total energies of the reactant and products are listed in Table 1. The values yield the dissociation reaction enthalpy of $\Delta H^{o}_{0K} = 0.05$ eV per formula unit (f.u.) for $CH_3NH_3PbI_3$ evaluated using Eq. (3). The result is within the range of theoretical values reported in the literature, including $\Delta H^{o}_{0K} = 0.1$ eV[22] and -0.06 eV[16]. The corresponding experimental value is $\Delta H^{o}_{300K} = -0.36$ eV[23], which is far too low to explain formability of this perovskite and needs further experimental verifications. The theoretical value of ΔH^{o}_{0K} contrasts sharply with the formation enthalpy of major solar cell compound materials, such as GaAs and CdTe, which is of the order of 0.8–1 eV/f.u.[24,25].

The poor chemical stability of $CH_3NH_3PbI_3$ is often attributed to the nearly vanishing value of ΔH[16,18]. In fact this only implies that the decomposition does not involve a heat exchange with environment. It is the finite temperature contribution to the chemical potential difference between reactants and products

$$\Delta\widetilde{\mu}^{o}_{T} = \sum_{i}^{\text{products}} n_i\widetilde{\mu}^{o}_{T}[i] - \sum_{j}^{\text{reactants}} n_j\widetilde{\mu}^{o}_{T}[j] \tag{4}$$

that remains overlooked in previous stability analysis[18,19,23]. Here $\widetilde{\mu}_T^{\circ}$ represents the final temperature correction to the chemical potential of spieces

$$\widetilde{\mu}_T^{\circ} = H_T^{\circ} - H_{0\,\mathrm{K}}^{\circ} - TS_T^{\circ}, \tag{5}$$

which is not captured in a bare DFT total energy. Although the extension of DFT calculations to finite temperatures is possible[26], it is computationally intensive. Therefore, NIST-JANAF thermochemical tables as well as other experimental resources were used to evaluate the final temperature correction using Eq. (5) (see Table 1 and references therein).

The final temperature correction to the Gibbs free energy of $CH_3NH_3PbI_3$ decomposition reaction

$$\Delta\widetilde{\mu}_T^{\circ} = \widetilde{\mu}_T^{\circ}(PbI_2) + \widetilde{\mu}_T^{\circ}(CH_3NH_3I) - \widetilde{\mu}_T^{\circ}(CH_3NH_3PbI_3) \tag{6}$$

amounts to $\Delta\widetilde{\mu}_{300\,\mathrm{K}}^{\circ} = 0.11\,\mathrm{eV/f.u.}$ The resultant Gibbs free energy difference in Eq. (2) is positive $\Delta G_{300\,\mathrm{K}}^{\circ} = 0.16\,\mathrm{eV/f.u.}$ indicating that the final temperature effects tend to stabilize the perovskite structure against spontaneous decomposition under standard conditions for temperature and pressure. However, the result should be taken with caution, since the uncertainty in reaction energies obtained with Perdew, Burke, and Ernzerhof (PBE)[27] exchange-correlation functional is of the order of $\pm 0.03\,\mathrm{eV/atom}$[28].

The thermodynamic characteristics of $CH_3NH_3PbI_3$ perovskites indicate that its chemical stability is fragile, and the balance can be easily shifted if the environment changes. A possible scenario that will be discussed here involves presence of a solvent. Unlike PbI_2 that has a limited solubility in water, the methylammonium iodide is highly soluble in water, which should be taken into account when calculating its chemical potential (see ref. 29, Chap. 8).

The actual chemical potential of an electrolyte

$$\mu_T \approx E_{\mathrm{total}} + \widetilde{\mu}_T^{\circ} + k_B T\ \ln(a_{\pm}) \tag{7}$$

can be significantly different from its value in the standard state depending on the activity coefficient $a_{\pm}$ of the solute[30]. The mean ionic activity $a_{\pm}$ of CH_3NH_3I solution

$$a_{\pm} = (\gamma_{\pm} c/c^{\circ})^2, \tag{8}$$

is determined by its molar concentration c relative to the concentration in standard state $c^{\circ} = 1\,\mathrm{M}$ and the mean ionic activity coefficient $\gamma_{\pm}$, which account for non-ideality of the solution. In a dilute solution limit, $c \ll 1\,\mathrm{M}$ and $\gamma_{\pm} \sim 1$, the chemical potential of aqueous CH_3NH_3I drops much below its value in the solid phase

$$\mu[CH_3NH_3I\,(\mathrm{aq})] \ll \mu[CH_3NH_3I\,(\mathrm{s})], \tag{9}$$

which shifts the balance in Eq. (1) to the right. Accordingly, the aqueous solubility of methylammonium iodide drives the dissociation of $CH_3NH_3PbI_3$ as previously suggested by Niu *et al.*[20]. The decomposition proceeds as long as the following condition is fulfilled

$$c < \frac{c^{\circ}}{\gamma_{\pm}} \exp\left(-\frac{\Delta G_T^{\circ}}{2k_B T}\right). \tag{10}$$

Using the value of $\Delta G_{300\,\mathrm{K}}^{\circ} = 0.16\,\mathrm{eV}$ and assuming $\gamma_{\pm} \sim 1$, it is possible to estimate the saturation concentration c_s of CH_3NH_3I dissolved in water at which further decomposition of $CH_3NH_3PbI_3$ is suppressed. Equation (10) yields $c_s \sim 50\,\mathrm{mM}$ (or ~8 g/L). Given the fact that the thickness of the absorbing material in perovskite solar cells is only $0.5\,\mu\mathrm{m}$[31], even a droplet of water is sufficient to destroy a device with the area of a several square centimeters.

Alternative absorber materials. The stability of hybrid lead halide perovskites can be improved by substituting iodine with more electronegative elements (bromine or chlorine)[23]. However, the associated increase of the band gap that exceeds 2 eV[22] limits the accessible power conversion efficiency when aiming for solar cell absorber materials. Therefore, we focus on perovskite structures of the family $XPbI_3$ and explore several alternatives for the cation $X = [NH_3OH]^+$, $[NH_3NH_2]^+$, $[PH_4]^+$, $[SbH_4]^+$, and $[SF_3]^+$. A solid solution of hydroxylammonium and hydrazinium ions were recently used in hybrid perovskite structures[32]. Phosphonium and particularly stibonium ions were theoretically predicted to produce more efficient photovoltaic materials when substituted for methylammonium in lead iodide-based perovskites due to the reduced band gap and improved effective mass[33]. Sulphur trifluoride represents an aprotic cation that can be beneficial in the context of resistance to degradation according to the mechanism discussed by Frost *et al.*[13]. Similar ionic volumes of $[SF_3^+]$ ($0.053\,\mathrm{nm}^3$) and $[CH_3NH_3]^+$ ($0.051\,\mathrm{nm}^3$) indicate proximity in size of both ions[34].

Unit cell volumes and band gaps of the corresponding perovskite structures are listed in Table 2. The band gaps were calculated without taking into account relativistic effects. This approach allows to minimize the error by taking advantage of an error cancelation between the band gap reduction due to spin-orbit coupling and its opening introduced by a port-DFT correction[35]. As a result, values of the band gap are only slightly overestimated (approximately 0.1 eV). The results indicate that small changes in the volume (less than 5%) lead to a sizeable change in the band gap. In contrast to group IV, III-V and II-VI semiconductors, the band gap in perovskite structures *increases* when the unit cell expands as Dittrich *et al.*[8] noticed. Out data clearly follow this trend with

Compound	V_0 (Å^3/f.u.)	$E_g^{DFT-GGA}$ (eV)	ΔH^o_{0K} (eV/f.u.)[a]
NH_3OHPbI_3	270	1.89	−0.25
$NH_3NH_2PbI_3$	274	1.80	−0.22
PH_4PbI_3	268	1.60	−0.18
SbH_4PbI_3	265	1.53	−0.11
β-$CH_3NH_3PbI_3$	263	1.67	+0.05
δ-$CsPbBr_3$	208	2.10	+0.37[b]
SF_3PbI_3	280	2.05	+0.87

Table 2. Dissociation reaction enthalpy ΔH^o_{0K} of perovskite structures presented together with volume of the unit cell V_0 and the band gap energy $E_g^{DFT-GGA}$ calculated self-consistently without taking into account the spin-orbit coupling. The generalized reaction for chemical decomposition is given by Eq. (1), except for SF_3PbI_3 that decomposes following the pathway in Eq. (11). [a]The positive value favours formation of the perovskite structure. [b]0.21 eV/f.u. is an alternative DFT result reported by Zhang *et al.*[16].

SbH_4PbI_3 being a favourite candidate for single-junction solar cells due to proximity of its band gap to the ideal value of 1.4 eV, which corresponds to the maximum efficiency in the Shockley-Queisser limit[36].

The chemical stability of perovskite structures in Table 2 was initially assessed by computing the decomposition reaction enthalpy ΔH^o_{0K}. In this calculation, we shall assume that all structures decompose following the pathway similar to Eq. (1) with the exception of SF_3PbI_3. Since there are no reports in the literature for SF_3I salt, the following decomposition route is considered

$$SF_3PbI_3 + 2H_2O \rightarrow PbI_2 + SO_2 + 3HF + HI. \quad (11)$$

This decomposition route also involves water, but in a different capacity from the degradation of $CH_3NH_3PbI_3$. Here water directly reacts with the perovskite.

Results for the decomposition reaction enthalpy calculated using Eq. (3) are given in Table 2, where the compounds are sorted in the order of increasing ΔH^o_{0K} (higher values favour stability of perovskites). Among all hybrid perovskites listed in Table 2, SF_3PbI_3 shows the highest decomposition reaction enthalpy indicating that the reaction (11) is strongly *endothermic*. All other hybrid perovskites with the negative reaction enthalpy can be rendered as unstable, including SbH_4PbI_3 with the promising band gap value.

The pseudocubic structures of SF_3PbI_3 perovskite is shown in Fig. 1 alongside with the pseudocubic structure of $CH_3NH_3PbI_3$. The band structure of both materials calculated taking into account spin-orbit coupling and a meta-GGA band gap correction are presented in Fig. 2. Both structures share qualitative similarities of the band dispersion. The band gap of SF_3PbI_3 is 0.4 eV higher than that for $CH_3NH_3PbI_3$. It is tempting to conclude that the new compound SF_3PbI_3 is stable due to the positive value of the enthalpy. It should be emphasized, however, that calculations of stability based on the formation enthalpy alone can lead to spurious results. If we take into account the final temperature correction $\tilde{\mu}^o_{300K}$ for the reactants and products in Table 1, we obtain the Gibbs free energy difference of $\Delta G^o_{300K} = -1.21$ eV. The negative value suggests that the reaction (11) can proceed spontaneously. This renders SF_3PbI_3 as being susceptible to reaction with moisture and warrants encapsulation as a protective provision against degradation.

Finally, it will be instructive to discuss the stability of an inorganic $CsPbBr_3$ perovskite. Unlike $CH_3NH_3PbI_3$, the decomposition reaction enthalpy of $CsPbBr_3$ is high (Table 2). Assuming that both compounds have the same magnitude of the final temperature contribution $\Delta\tilde{\mu}^o_{300K}$ to the free energy, one would expect the free energy of $CsPbBr_3$ to be approximately 0.5 eV/f.u. *lower* than that for decomposition products ($PbBr_2$ and CsBr) indicating strong chemical stability of $CsPbBr_3$ against spontaneous decomposition. However, it is found experimentally that the performance of $CsPbBr_3$-based solar cells (not encapsulated) decays over time, although slower than $CH_3NH_3PbI_3$-based devices[37]. This observation reveals susceptibility of both perovskite structures to the reaction with moisture, despite of the high reaction enthalpy of $CsPbBr_3$ and lack of proton-donating groups. We believe that the aqueous solubility of CsBr has some significance for explaining this effect. The slow degradation rate of $CsPbBr_3$ can be attributed to the greater value of ΔG^o_{300K}, which translates into a much lower saturation concentration of CsBr $c_s \sim 60\ \mu$M as compared to $c_s \sim 50$ mM for CH_3NH_3I (see discussion in the preceding subsection).

Conclusions

The performance of $CH_3NH_3PbI_3$ perovskites solar cells deteriorates when exposed to environmental factors, such as moisture and sunlight. This remains the main barrier on the way to their commercialization. The ability to assess stability of solar cell absorber materials using first principle calculations is an important attribute for design of new materials. We showed that the instability of perovskites can be captured using DFT total energy calculations for reactants and products augmented with additional thermodynamic data to account for finite temperature effects. The finite temperature effects play a minor role stabilizing the perovskite structure when products of the decomposition reaction are solids. However, the finite temperature contribution to the Gibbs free energy of the degradation reaction becomes crucially important in the case of when products of the decomposition are aqueous solutions or gases.

Our calculations suggest that the $CH_3NH_3PbI_3$ structure can be stable against spontaneous decomposition, provided it is isolated from environmental factors. The situation changes drastically in the presence of water. The

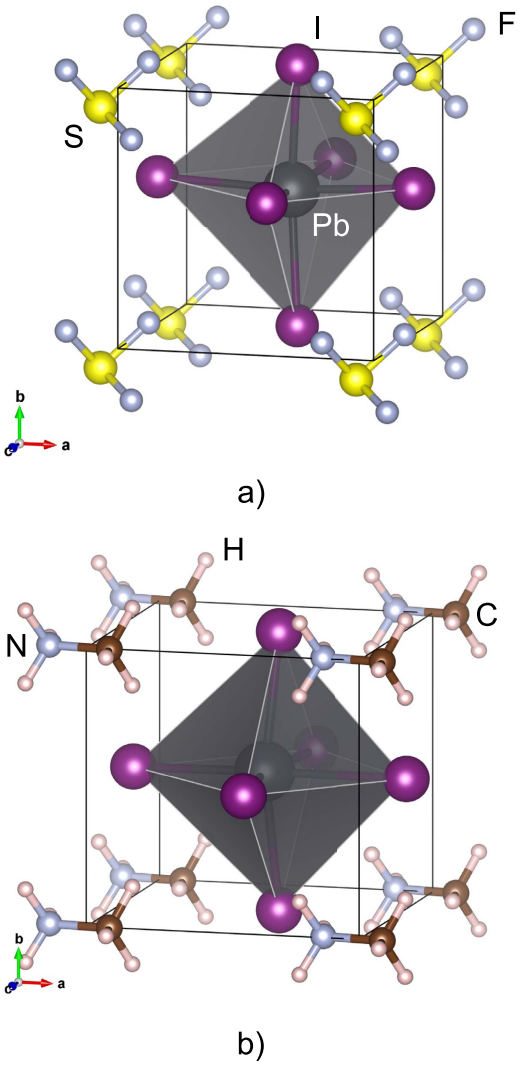

Figure 1. Structure of pseudocubic SF_3PbI_3 (**a**) and $CH_3NH_3PbI_3$ (**b**).

aqueous solubility of the CH_3NH_3I salt lowers its chemical potential relative to the solid phase, especially in a dilute limit. This property favours decomposition of $CH_3NH_3PbI_3$ in the moist environment. Therefore, a limited solubility of the decomposition reaction products is anticipated to improve structural stability. Generalizing this result to other perovskites, the aqueous solubility of $HC(NH_2)_2I$, SbH_4I, and CsBr undermines stability of the corresponding perovskite structures.

In a search for alternative perovskites, NH_3OHPbI_3, $NH_3NH_2PbI_3$, PH_4PbI_3, SbH_4PbI_3, $CsPbBr_3$, and SF_3PbI_3 compounds were investigated. NH_3OHPbI_3, $NH_3NH_2PbI_3$, PH_4PbI_3, and SbH_4PbI_3 were concluded unstable due to the low formation enthalpy. The $CsPbBr_3$ structure is prone to degradation in moist conditions, in spite of the favourable formation enthalpy, due to solubility of CsBr. Straightforward comparison of DFT total energies of reactants and products provides an argument in favour of the chemical stability for the SF_3PbI_3 structure. The predicted value for the energy band gap of this new compound is approximately 2 eV. However, more detailed analysis that incorporates finite temperature effects renders the material unstable to decomposition in a moist environment thus signifying the importance of those effects for future analysis.

Computational details. The first-principles electronic structure calculations were carried out using DFT[38]. Two implementations were employed. A projector augmented wave (PAW) method[39,40] implemented in the ABINIT package[41–43] was utilized for the structural optimization and calculations of the chemical stability. The band structure calculations were performed in the Wien2k package[44] based on a full potential linear augmented plane wave method.

Structure optimization. The $CH_3NH_3PbI_3$ perovskite is known to exist in three different polymorphs[5,45]: orthorhombic, tetragonal, and cubic. A tetragonal β-phase is stable at room temperature and was used in these calculations. A pseudocubic structure was used to represent SF_3PbI_3, NH_3OHPbI_3, $NH_3NH_2PbI_3$, PH_4PbI_3, and SbH_4PbI_3. An orthorhombic (Pnma) structure was chosen to represent δ-$CsPbBr_3$. Optimization of lattice parameters was carried out in conjunction with relaxation of internal degrees of freedom for all structures studied here. The structure was considered optimized when the magnitude of Hellmann-Feynman forces acting on atoms

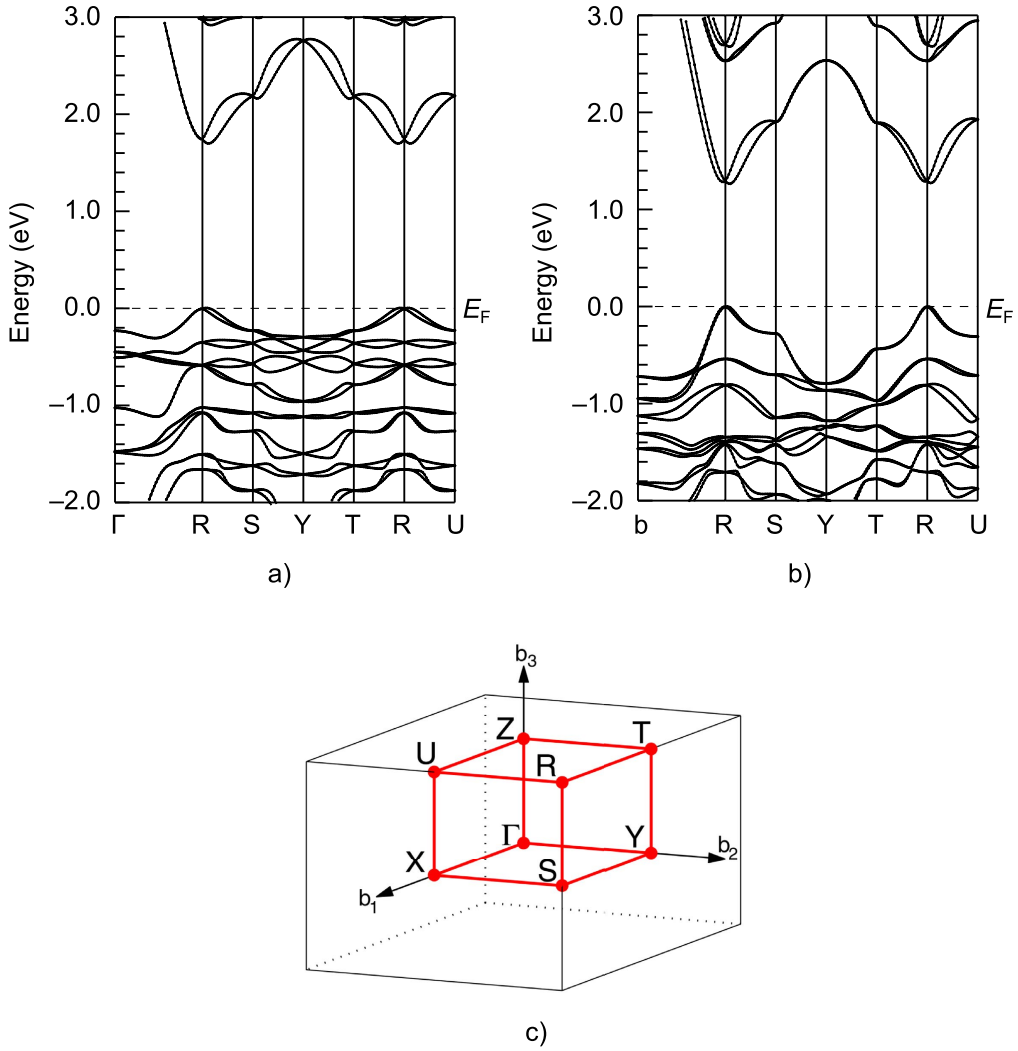

Figure 2. Band structure of pseudocubic SF_3PbI_3 (**a**) and $CH_3NH_3PbI_3$ (**b**) calculated along the path between high-symmetry points in the Brillouin zone (**c**) taking into account spin-orbit coupling and non-local exchange correction. The origin of the energy scale is set at the Fermi energy E_F. Labels of the high-symmetry point in the Brillouin zone correspond to an orthorhombic lattice[53].

dropped below 0.5 mHa/Bohr and components of the stress tensor were less than 1 μHa/Bohr^3. The Brillouin zone was sampled using an unshifted mesh with the density one k-point per every 0.01 Bohr^{-1} length of each reciprocal lattice vector. The cutoff energy for a plane wave expansion was set at 15 Ha.

Standard structures of solid PbI_2 (hexagonal, space group 164 ($P\bar{3}m1$)m1)), PbF_2 (cubic, space group 225 ($Fm\bar{3}m$)) and $PbBr_2$ (orthorhombic, space group 62 (Pbnm)) were used to represent possible reactants. The structure of CH_3NH_3I undergoes several phase transitions with increasing temperature[46]. A tetragonal α'-phase (space group 129 (P4/nmm)), which is stable at room temperature, resembles a rock-salt ionic structure[47]. The total energy of water was derived from its natural I_h solid structure (hexagonal, space group 194 ($P6_3/mmc$) ref. 48). Structures of NH_3OHI, NH_3NH_2I, PH_4I, and SbH_4I were derived using CsCl structure as a prototype. All structures were fully optimized as describe in the preceding paragraph (without constrains to the geometry).

Gaseous phases were modelled as an individual molecule surrounded by 30 Bohrs of vacuum. The internal degrees of freedom were relaxed. Only Γ-point was used in the Brillouin zone.

Perdew, Burke, and Ernzerhof[27] version of the generalized gradient approximation was chosen for the exchange correlation functional due to its superior accuracy in predicting cohesive properties of solids and molecules.

Garrity, Bennett, Rabe, and Vanderbilt[49] GBRV (v1.5) PAW pseudopotentials were employed for all elements. VESTA 3 package was used for visualization of atomic structure[50]. Structure files of all perovskite compounds and non-trivial salts are included in the supplementary information in a cif-format.

Band structure. The band structure of pseudocubic SF_3PbI_3 and $CH_3NH_3PbI_3$ were calculated with the Wien2k package[44] using a full potential linear augmented plane wave method. The Brillouin zone was sampled using $6 \times 6 \times 6$ Monkhorst and Pack[51] mesh. The muffin-tin radii R_{MT} where set to 0.62, 1.16, 1.22, 1.38, 1.47, 2.2,

and 2.2 Bohr for H, N, C, S, F, I, and Pb respectively. The cutoff energy of −6 Ry was used to separates valence and core electrons. The product $R_{\min}^{\mathrm{MT}} K_{\max}$, which determines the accuracy of a plane wave expansion of the wave function, was set at the values of 3.5 and 6 for $CH_3NH_3PbI_3$ and SF_3PbI_3 compounds, respectively. The low $R_{\min}^{\mathrm{MT}} K_{\max}$ for $CH_3NH_3PbI_3$ is due to a small size of the muffin-tin sphere around hydrogen atoms. Optimized lattice parameters and atomic positions from ABINIT calculations were used. The Tran-Blaha modified Becke-Johnson (TBmBJ) potential[52] was applied in order to overcome shortcomings of DFT semilocal exchange correlation functions in predicting band gaps of insulators.

References

1. M. M. Lee, J. Teuscher, T. Miyasaka, T. N. Murakami & H. J. Snaith. "Efficient hybrid solar cells based on meso-superstructured organometal halide perovskites". *Science* **338,** 643–647 (2012).
2. Nam-Gyu Park. "Organometal perovskite light absorbers toward a 20% efficiency low-cost solid-state mesoscopic solar cell". *J. Phys. Chem. Lett.* **4,** 2423–2429 (2013).
3. H. S. Jung & N. G. Park. "Perovskite solar cells: From materials to devices". *Small* **11,** 10–25 (2014).
4. Woon Seok Yang *et al.* "High-performance photovoltaic perovskite layers fabricated through intramolecular exchange". *Science* **348,** 1234–1237 (2015).
5. Constantinos C. Stoumpos, Christos D. Malliakas & Mercouri G. Kanatzidis. "Semiconducting tin and lead iodide perovskites with organic cations: Phase transitions, high mobilities, and near-infrared photoluminescent properties". *Inorg. Chem.* **52,** 9019–9038 (2013).
6. Jingbi You *et al.* "Low-temperature solution-processed perovskite solar cells with high efficiency and flexibility". *ACS Nano* **8,** 1674–1680 (2014).
7. Yasuhiro Yamada *et al.* "Near-band-edge optical responses of solution-processed organic-inorganic hybrid perovskite $CH_3NH_3PbI_3$ on mesoporous TiO_2 electrodes". *Appl. Phys. Express* **7,** 032302 (2014).
8. Thomas Dittrich *et al.* "Temperature dependence of the band gap of CH3NH3PbI3 stabilized with PMMA: A modulated surface photovoltage study". *J. Phys. Chem. C* **119,** 23968–23972 (2015).
9. Jeffrey A. Christians, Pierre A. Miranda Herrera & Prashant V. Kamat. "Transformation of the excited state and photovoltaic efficiency of CH3NH3PbI3 perovskite upon controlled exposure to humidified air". *J. Am. Chem. Soc.* **137,** 1530–1538 (2015).
10. Sarah Wozny *et al.* "Controlled humidity study on the formation of higher efficiency formamidinium lead triiodide-based solar cells". *Chem. Mater.* **27,** 4814–4820 (2015).
11. Bertrand Philippe *et al.* "Chemical and electronic structure characterization of lead halide perovskites and stability behavior under different exposures—a photoelectron spectroscopy investigation". *Chem. Mater.* **27,** 1720–1731 (2015).
12. Jinli Yang, Braden D. Siempelkamp, Dianyi Liu & Timothy L. Kelly. "Investigation of CH3NH3PbI3 degradation rates and mechanisms in controlled humidity environments using *in situ* techniques". *ACS Nano* **9,** 1955–1963 (2015).
13. Jarvist M. Frost *et al.* "Atomistic origins of high-performance in hybrid halide perovskite solar cells". *Nano Lett.* **14,** 2584–2584 (2014).
14. Edoardo Mosconi, Jon M. Azpiroz & Filippo De Angelis. "Ab initio molecular dynamics simulations of methylammonium lead iodide perovskite degradation by water". *Chem. Mater.* **27,** 4885–4892 (2015).
15. Linghai Zhang & Patrick H.-L. Sit. "Ab initio study of interaction of water, hydroxyl radicals, and hydroxide ions with CH3NH3PbI3 and CH3NH3PbBr3 surfaces". *J. Phys. Chem. C* **119,** 22370–22378 (2015).
16. Yue-Yu Zhang *et al.* "Intrinsic instability of the hybrid halide perovskite semiconductor CH3NH3PbI3". arXiv preprint arXiv:1506.01301 (2015).
17. Yu Han *et al.* "Degradation observations of encapsulated planar CH3NH3PbI3 perovskite solar cells at high temperatures and humidity". *J. Mater. Chem. A* **3,** 8139–8147 (2015).
18. Wan-Jian Yin, Tingting Shi & Yanfa Yan. "Unusual defect physics in CH3NH3PbI3 perovskite solar cell absorber". *Appl. Phys. Lett.* **104,** 063903 (2014).
19. Jun Haruyama, Keitaro Sodeyama, Liyuan Han & Yoshitaka Tateyama. "Termination dependence of tetragonal CH3NH3PbI3 surfaces for perovskite solar cells". *J. Phys. Chem. Lett.* **5,** 2903–2909 (2014).
20. Guangda Niu *et al.* "Study on the stability of CH3NH3PbI3 films and the effect of post-modification by aluminum oxide in all-solid-state hybrid solar cells". *J. Mater. Chem. A* **2,** 705–710 (2014).
21. David Sholl & Janice A. Steckel. *Density functional theory: a practical introduction* (John Wiley & Sons, 2011).
22. Andrei Buin *et al.* "Halide-dependent electronic structure of organolead perovskite materials". *Chem. Mater.* **27,** 4405–4412 (2015).
23. G. P. Nagabhushana, Radha Shivaramaiah & Alexandra Navrotsky. "Direct calorimetric verification of thermodynamic instability of lead halide hybrid perovskites". *Proc. Natl. Acad. Sci. USA*, 201607850 (2016).
24. G. Zollo & R. M. Nieminen. "Small self-interstitial clusters in GaAs". *J. Phys.: Condens. Matter* **15,** 843 (2003).
25. S. H. Wei & S. B. Zhang. "Theoretical study of doping limits of CdTe". In *NCPV Program Review Meeting* 14–17 (2001).
26. Atsushi Togo, Laurent Chaput, Isao Tanaka & Gilles Hug. "First-principles phonon calculations of thermal expansion in Ti_3SiC_2, Ti_3AlC_2, and Ti_3GeC_2". *Phys. Rev. B* **81,** 174301 (2010).
27. John P. Perdew, Kieron Burke & Matthias Ernzerhof. "Generalized gradient approximation made simple". *Phys. Rev. Lett.* **77,** 3865 (1996).
28. Geoffroy Hautier *et al.* "Accuracy of density functional theory in predicting formation energies of ternary oxides from binary oxides and its implication on phase stability". *Phys. Rev. B* **85,** 155208 (2012).
29. Margaret Robson Wright. *An Introduction to Aqueous Electrolyte Solutions* (John Wiley & Sons, 2007).
30. Mike J. Blandamer, Jan B. F. N. Engberts, Peter T. Gleeson & Joao Carlos R. Reis. "Activity of water in aqueous systems; a frequently neglected property". *Chem. Soc. Rev.* **34,** 440–458 (2005).
31. Dianyi Liu, Mahesh K. Gangishetty & Timothy L. Kelly. "Effect of CH3NH3PbI3 thickness on device efficiency in planar heterojunction perovskite solar cells". *J. Mater. Chem. A* **2,** 19873–19881 (2014).
32. Gregor Kieslich *et al.* "Tuneable mechanical and dynamical properties in the ferroelectric perovskite solid solution [NH3NH2]1-x[NH3OH]xZn(HCOO)3". *Chem. Sci.* **7,** 5108–5112 (2016).
33. Marina R. Filip, Carla Verdi & Feliciano Giustino. "GW band structures and carrier effective masses of CH3NH3PbI3 and hypothetical perovskites of the type APbI3: A = NH4, PH4, AsH4, and SbH4". *J. Phys. Chem. C* **119,** 25209–25219 (2015).
34. H. Donald B. Jenkins, Helen K. Roobottom, Jack Passmore & Leslie Glasser. "Relationships among ionic lattice energies, molecular (formula unit) volumes, and thermochemical radii". *Inorg. Chem.* **38,** 3609–3620 (1999).
35. Edoardo Mosconi *et al.* "First-principles modeling of mixed halide organometal perovskites for photovoltaic applications". *J. Phys. Chem. C* **117,** 13902–13913 (2013).
36. Sven Rühle. "Tabulated values of the shockley–queisser limit for single junction solar cells". *Solar Energy* **130,** 139–147 (2016).
37. Michael Kulbak *et al.* "Cesium enhances long-term stability of lead bromide perovskite-based solar cells". *J. Phys. Chem. Lett.* **7,** 167–172 (2015).
38. W. Kohn & L. J. Sham. "Self-consistent equations including exchange and correlation effects". *Phys. Rev.* **140,** A1133 (1965).
39. G. Kresse & D. Joubert. "From ultrasoft pseudopotentials to the projector augmented-wave method". *Phys. Rev. B* **59,** 1758 (1999).

40. Marc Torrent *et al.* "Implementation of the projector augmented-wave method in the abinit code: Application to the study of iron under pressure". *Comp. Mater. Sci.* **42,** 337–351 (2008).
41. X. Gonze *et al.* "First-principles computation of material properties: the abinit software project". *Comp. Mater. Sci.* **25,** 478 (2002).
42. X. Gonze *et al.* "A brief introduction to the abinit software package". *Zeit. Kristallogr.* **220,** 558 (2005).
43. X. Gonze *et al.* "Abinit: First-principles approach to material and nanosystem properties". *Comput. Phys. Commun.* **180,** 2582–2615 (2009).
44. P. Blaha, K. Schwarz, G. K. H. Madsen, D. Kvasnicka & J. Luitz. *Wien2k*: *An Augmented Plane Wave + Local Orbitals Program for Calculating Crystal Properties* (Karlheinz Schwarz, Techn. Universität Wien, Austria, 2001).
45. Tom Baikie *et al.* "Synthesis and crystal chemistry of the hybrid perovskite (CH3NH3)PbI3 for solid-state sensitised solar cell applications". *J. Mater. Chem. A* **1,** 628 (2013).
46. Osamu Yamamuro, Masaharu Oguni, Takasuke Matsuo & Hiroshi Suga. "PT phase relations of methylammonium halides". *Thermochim. Acta* **98,** 327–338 (1986).
47. Hiroyuki Ishida *et al.* "Exafs study on the phase transition (phase α-δ) in CH3NH3I". *Zeitschrift für Naturforschung A* **50,** 876–880 (1995).
48. Andrew D. Fortes *et al.* "No evidence for large-scale proton ordering in Antarctic ice from powder neutron diffraction". *J. Chem. Phys.* **120,** 11376–11379 (2004).
49. Kevin F. Garrity, Joseph W. Bennett, Karin M. Rabe & David Vanderbilt. "Pseudopotentials for high-throughput dft calculations". *Comp. Mater. Sci.* **81,** 446–452 (2014).
50. Koichi Momma & Fujio Izumi. "VESTA3 for three-dimensional visualization of crystal, volumetric and morphology data". *J. Appl. Crystallogr.* **44,** 1272–1276 (2011).
51. H. J. Monkhorst & J. D. Pack. "Special points for brillouin-zone integrations". *Phys. Rev. B* **13,** 5188 (1976).
52. Fabien Tran & Peter Blaha. "Accurate band gaps of semiconductors and insulators with a semilocal exchange-correlation potential". *Phys. Rev. Lett.* **102,** 226401 (2009).
53. Wahyu Setyawan & Stefano Curtarolo. "High-throughput electronic band structure calculations: Challenges and tools". *Comp. Mater. Sci.* **49,** 299–312 (2010).
54. Noriko Onoda-Yamamuro, Takasuke Matsuo & Hiroshi Suga. "Calorimetric and IR spectroscopic studies of phase transitions in methylammonium trihalogenoplumbates (II)". *J. Phys. Chem. Solids* **51,** 1383–1395 (1990).
55. M. W. Chase. *NIST-JANAF Thermochemical Tables* 4th Edition (American Institute of Physics, 1998).
56. O. Yamamuro, M. Oguni, T. Matsuo & H. Suga. "Calorimetric and dilatometric studies on the phase transitions of crystalline CH3NH3I". *J. Chem. Thermodynamics* **18,** 939–954 (1986).
57. W. F. Giauque & J. W. Stout. "The entropy of water and the third law of thermodynamics. The heat capacity of ice from 15 to 273 °K". *J. Am. Chem. Soc.* **58,** 1144–1150 (1936).
58. A. Poglitsch & D. Weber. "Dynamic disorder in methylammoniumtrihalogenoplumbates (ii) observed by millimeter-wave spectroscopy". *J. Chem. Phys.* **87,** 6373–6378 (1987).
59. Wan-Jian Yin, Yanfa Yan & Su-Huai Wei. "Anomalous alloy properties in mixed halide perovskites". *J. Phys. Chem. Lett.* **5,** 3625–3631 (2014).
60. O. Madelung, U. Rössler & M. Schulz. eds. "Lead diiodide (PbI2) crystal structure, lattice parameters, thermal expansion". In *Non-Tetrahedrally Bonded Elements and Binary Compounds I*, 1–3 (Springer Berlin Heidelberg, Berlin, Heidelberg, 1998).
61. Sterling B. Hendricks. "V. The crystal structures of the monomethyl ammonium halides". *Zeitschrift für Kristallographie-Crystalline Materials* **67,** 106–118 (1928).
62. K. Röttger *et al.* "Lattice constants and thermal expansion of H2O and D2O ice Ih between 10 and 265 K". *Acta Crystallogr. Sect. B* **50,** 644–648 (1994).

Acknowledgements

Funding is provided by the Natural Sciences and Engineering Research Council (NSERC) of Canada under the Discovery Grant Program RGPIN-2015-04518. ET would like to acknowledge the financial support from the NSERC Undergraduate Student Research Awards program. The work is performed using computational resources of Thunder Bay Regional Research Institute, Lakehead University, and Compute Canada (Calcul Quebec).

Author Contributions

E.T. performed majority of D.F.T. calculations and proposed SF_3PbI_3 structure. C.Z. performed D.F.T. calculations of CH_3NH_3I and performed thermodynamic analysis. O.R. wrote the main manuscript text and prepared figures. All authors reviewed the manuscript.

Additional Information

Supplementary information accompanies this paper at http://www.nature.com/srep

Competing financial interests: The authors declare no competing financial interests.

How to cite this article: Tenuta, E. *et al.* Thermodynamic origin of instability in hybrid halide perovskites. *Sci. Rep.* **6**, 37654; doi: 10.1038/srep37654 (2016).

Publisher's note: Springer Nature remains neutral with regard to jurisdictional claims in published maps and institutional affiliations.